Journal of Engineering Mathematics **26**: 493–508, 1992.

Numerical and asymptotic solutions for the thermal wall jet

P.G. DANIELS and R.J. GARGARO
Department of Mathematics, City University, Northampton Square, London EC1V 0HB, UK

Received 31 October 1991; accepted in revised form 16 March 1992

Abstract. This paper considers the evolution of the velocity and temperature fields within a jet of fluid on a thermally insulated wall. Numerical solutions are obtained for a range of Prandtl numbers and for a class of initial velocity and temperature profiles relevant to intrusion jets observed in certain thermal cavity flows. Numerical results are compared with asymptotic solutions which describe the initial structure of the jet and its subsequent diffusion at large distances downstream.

1. Introduction

The development of a two-dimensional jet flow along a rigid wall was considered theoretically by Glauert [1]. Using a boundary-layer approximation he showed that the jet would satisfy an integral property equivalent to conservation of the flux of momentum flux and established the similarity form into which the jet would evolve downstream. This showed that the width of the jet grows like $x^{*3/4}$ and that its speed decreases like $x^{*-1/2}$ where x^* is the downstream co-ordinate. Such wall jets occur in a variety of situations, in some cases with an associated thermal field which is also of interest.

One example is in the area of thermally-driven cavity flows, which are widely studied in connection with crystal-growth processes (Hurle [2]), cooling systems (Boyack and Kearney [3]), solar-energy collectors (Bejan and Rossie [4]) and a variety of geophysical phenomena. In shallow, laterally-heated cavities where natural convection is generated by maintaining the end-walls at different constant temperatures (Cormack, Leal and Imberger [5], Daniels, Blythe and Simpkins [6]) the flow consists primarily of upward motion near the hot end-wall and downward motion near the cold end-wall, the main single-cell circulation being completed across the central region by a two-way flow parallel to the horizontal boundaries. At high Rayleigh numbers the vertical motion near the end-walls is compressed into thin boundary layers which transport fluid to the base of the cold wall and the top of the hot wall and from there it issues into the central region in the form of 'intrusion' jets. These have been studied experimentally by Bejan, Al-Homoud and Imberger [7] and Simpkins and Chen [8] and more recently transient features of the motion have been investigated by Schladow, Patterson and Street [9] and Patterson and Armfield [10]. One model of the steady-state end-region flow (Daniels, Blythe and Simpkins [11]) suggests that in very long cavities the motion in these intrusion jets is initially unaffected by the thermal field, being generated by the mass-flux conveyed in the vertical boundary layers. The thermal field itself is generated by the non-uniformity in temperature within the vertical boundary layer, where the solution can be approximated by the well-known similarity form for a heated vertical plate (Pohlhausen [12], Squire, see Goldstein [13]). This leads to the development of the horizontal intrusions with initial velocity and temperature profiles that correspond to a stably-stratified jet flow. These profiles are Prandtl-number dependent, being obtained from

the similarity solution of the vertical boundary-layer equations. It is not proposed to consider here the precise manner in which the jet flow turns the corner of the cavity, which is a problem of some complexity. Possible mechanisms for separation ahead of the corner and a related eddy-structure have been advanced by Smith and Duck [14].

The plan of the paper is as follows. In Section 2 the governing equations and boundary conditions are described and these lead to an integral property of the velocity field first established in [1] and a corresponding result for the temperature field. In Section 3 asymptotic results are described for small and large values of the non-dimensional downstream co-ordinate x. At small values of x a lack of smoothness between the initial profiles and the wall conditions gives rise to singular expansions and the temperature field, in particular, undergoes rapid adjustment in an inner region adjacent to the thermally-insulated wall. At large values of x the similarity form for the velocity field obtained in [1] is extended to yield a corresponding result for the temperature field, confirming that the temperature across the jet becomes uniform as $x \to \infty$. Numerical computations of the velocity and temperature fields in the jet are described in Section 4. These use a sophisticated finite-difference scheme based on the asymptotic structure of the solution and results are obtained for a wide range of Prandtl numbers. A summary and discussion of the results is given in Section 5.

2. Formulation

A two-dimensional thermal jet flow occurs along a rigid, thermally insulated plane $z^* = 0$ and is generated at $x^* = 0$ by velocity and temperature profiles u^* and T^* varying on a length scale $z^* = h$ and of magnitude U and ΔT^* respectively. Assuming that the Reynolds number $\mathrm{Re} = Uh/\nu$ is large, where ν is the kinematic viscosity of the fluid, and that effects of compressibility and buoyancy may be neglected, the Navier–Stokes and thermal energy equations reduce to the non-dimensional form

$$\frac{\partial u}{\partial x} + \frac{\partial w}{\partial z} = 0\,, \tag{1}$$

$$u\frac{\partial u}{\partial x} + w\frac{\partial u}{\partial z} = \frac{\partial^2 u}{\partial z^2}\,, \tag{2}$$

$$u\frac{\partial T}{\partial x} + w\frac{\partial T}{\partial z} = \frac{1}{\sigma}\frac{\partial^2 T}{\partial z^2}\,. \tag{3}$$

Here $(x^*, z^*) = h(\mathrm{Re}\, x, z)$, $(u^*, w^*) = U(u, \mathrm{Re}^{-1} w)$, $T^* = \Delta T^* T$ and

$$\sigma = \nu/\kappa \tag{4}$$

is the Prandtl number of the fluid, where κ is the thermal diffusivity. A stream function ψ is introduced, with

$$u = \frac{\partial \psi}{\partial z}\,, \qquad w = -\frac{\partial \psi}{\partial x}\,. \tag{5}$$

At the wall the boundary conditions are

$$u = w = \frac{\partial T}{\partial z} = 0 \quad (z = 0)\,, \tag{6}$$

while at the edge of the jet it is required that

$$u \to 0\,, \quad T \to 1 \qquad (z \to \infty)\,, \tag{7}$$

assuming ΔT^* to be taken as the ambient temperature. As explained in the Introduction, the initial profiles at $x = 0$ are to be provided by the solution

$$\psi = F_0(z)\,, \qquad T = G_0(z) \tag{8}$$

of the vertical boundary-layer system

$$F_0''' + \tfrac{3}{4} F_0 F_0'' - \tfrac{1}{2} F_0'^2 + \sigma^{-1}(1 - G_0) = 0\,, \tag{9}$$

$$G_0'' + \tfrac{3}{4} \sigma F_0 G_0' = 0\,, \tag{10}$$

$$F_0 = F_0' = G_0 = 0 \quad (z = 0)\,, \qquad F_0' \to 0\,, \quad G_0 \to 1 \quad (z \to \infty)\,, \tag{11}$$

(see [11]–[13]). Numerical solutions of this system were first obtained by Ostrach [15] and here a finite-difference Newton iteration was used to obtain profiles F_0 and G_0 for a range of Prandtl numbers. Details of the scheme are given by Gargaro [16]. Solutions are shown in Figs 1–2 and at large Prandtl numbers the results compare well with the asymptotic analysis of Kuiken [17]. As $z \to 0$ the profiles F_0 and G_0 have the forms

$$F_0 = \alpha z^2 - \frac{1}{6\sigma} z^3 + \frac{\beta}{24\sigma} z^4 + \cdots\,, \tag{12}$$

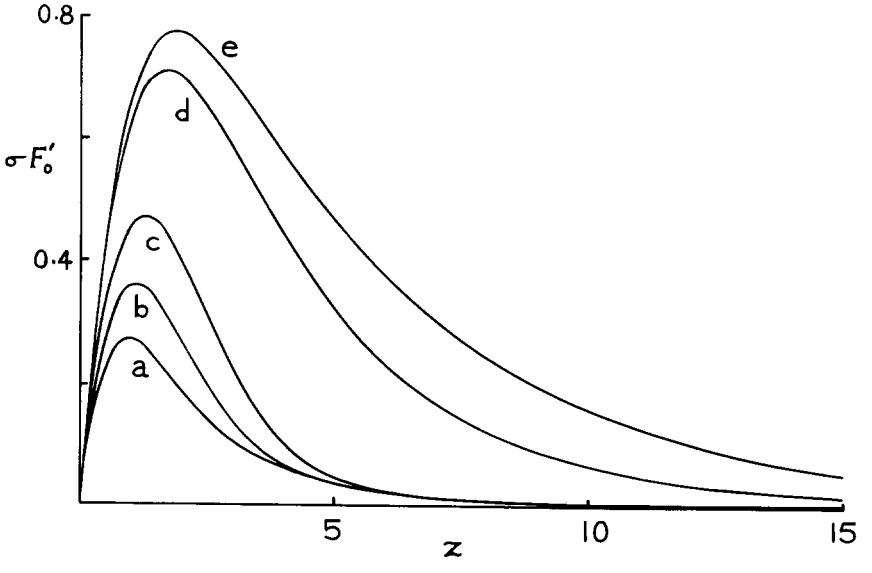

Fig. 1. Initial velocity profile for Prandtl numbers: (a) 0.028; (b) 0.1; (c) 0.72; (d) 8.1; (e) 17.2.

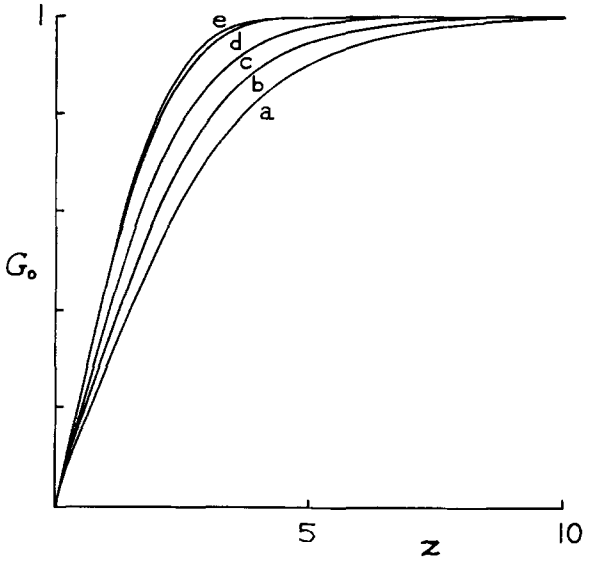

Fig. 2. Initial temperature profile for Prandtl numbers: (a) 0.028; (b) 0.1; (c) 0.72; (d) 8.1; (e) 17.2.

$$G_0 = \beta z - \tfrac{1}{16}\sigma\alpha\beta z^4 + \cdots , \tag{13}$$

and values of the coefficients α and β are given in Table 1.

The system (1)–(8) possesses two integral properties, the first of which was derived in [1] and expresses the fact that the flux of momentum flux is constant at any cross-section of the jet:

$$\int_0^\infty u\left(\int_z^\infty u^2\,\mathrm{d}z\right)\mathrm{d}z = P , \tag{14}$$

where P is a constant which can be determined from the initial velocity profile by substitution of (8) into (14). Since no heat can escape through the wall or at the edge of the jet the heat flux is also constant at any cross-section of the jet:

$$\int_0^\infty \psi \frac{\partial T}{\partial z}\,\mathrm{d}z = Q , \tag{15}$$

where Q is a constant which can be determined from the initial profiles (8). Values of P and Q are given in Table 1 for a range of Prandtl numbers.

Table 1. Properties of initial profiles

σ	α	β	P	Q
0.1	3.416	0.289	39.63	3.858
0.72	0.612	0.387	0.6487	0.717
8.1	0.065	0.461	0.0043	0.076
17.2	0.031	0.478	0.0009	0.037

3. Asymptotic solutions

In this section solutions of (1)–(8) are considered for small and large values of the streamwise co-ordinate x. Although the initial velocity profile (8) is consistent with the wall conditions (6) the velocity field is not regular at $x = 0$. This is because the initial profile F_0 generated by thermal effects within the vertical boundary layer has the property that $F_0'''(0) \neq 0$ and this is inconsistent with the isothermal jet equation (2) which implies that $\partial^3\psi/\partial z^3 = 0$ at $z = 0$ for all values of x. This leads to an expansion for the velocity field as $x \to 0+$ consisting of an outer region where

$$\psi = F_0(z) + x^{2/3}F_1(z) + \cdots, \tag{16}$$

and an inner viscous region where

$$\psi = x^{2/3}f_0(\eta) + xf_1(\eta) + \cdots, \tag{17}$$

and $\eta = z/x^{1/3}$. Substitution of (17) into (1) gives, at leading order,

$$f_0''' + \tfrac{2}{3}f_0f_0'' - \tfrac{1}{3}f_0'^2 = 0, \tag{18}$$

and this is to be solved subject to the conditions

$$f_0 = f_0' = 0 \quad (\eta = 0), \qquad f_0 \sim \alpha\eta^2 \quad (\eta \to \infty), \tag{19}$$

obtained from (6) and from matching with the small-z expansion of the outer form (16) provided by (12). The required solution is

$$f_0 = \alpha\eta^2. \tag{20}$$

At second order f_1 is found to satisfy the equation

$$f_1''' + \tfrac{2}{3}\alpha\eta^2 f_1'' - 2\alpha\eta f_1' + 2\alpha f_1 = 0, \tag{21}$$

with boundary conditions

$$f_1 = f_1' = 0 \quad (\eta = 0), \qquad f_1 \sim -\eta^3/6\sigma \quad (\eta \to \infty). \tag{22}$$

The solution is given by

$$f_1(\eta) = (2\alpha\sigma)^{-1}\tilde{f}_1(\tilde{\eta}), \qquad \eta = (2\alpha)^{-1/3}\tilde{\eta}, \tag{23}$$

where

$$\tilde{f}_1 = 1 - \tfrac{1}{6}\tilde{\eta}^3 + (I'(0)\tilde{\eta} - I(\tilde{\eta}))/I(0) \tag{24}$$

and

$$I(\tilde{\eta}) = \tilde{\eta}\int_{\tilde{\eta}}^{\infty}\left(u + \frac{3}{u^2}\right)\left(\int_u^{\infty}\frac{v}{(3+v^3)^2}\,e^{-v^3/9}\,dv\right)du. \tag{25}$$

A solution was also obtained by direct numerical integration using a Runge–Kutta scheme and is shown in Fig. 3. As $\eta \to \infty$,

$$f_1 \sim -\frac{1}{6\sigma}\eta^3 + a\eta\,, \tag{26}$$

where $a = -1.43/\sigma(2\alpha)^{2/3}$. The linear term in η produces a reaction in the outer region where the term $F_1(z)$ must now vanish as $z \to 0$ and satisfy $F_1'(0) = a$. Substitution of (16) into (2) shows that F_1 is proportional to F_0' and so the required solution is

$$F_1 = aF_0'/2\alpha\,. \tag{27}$$

The temperature field adopts a similar double structure as $x \to 0$ except that the discontinuity in wall heat transfer leads to a more severe non-uniformity. In the outer region

$$T = G_0(z) + x^{2/3}G_1(z) + \cdots \quad (x \to 0+)\,, \tag{28}$$

while in the inner region

$$T = x^{1/3}g_0(\eta) + x^{2/3}g_1(\eta) + \cdots \quad (x \to 0+)\,. \tag{29}$$

Substitution into (3) shows that g_0 satisfies

$$g_0'' + \tfrac{2}{3}\alpha\sigma\eta^2 g_0' - \tfrac{2}{3}\alpha\sigma\eta g_0 = 0 \tag{30}$$

and this is to be solved subject to the conditions

$$g_0' = 0 \quad (\eta = 0)\,, \qquad g_0 \sim \beta\eta \quad (\eta \to \infty)\,, \tag{31}$$

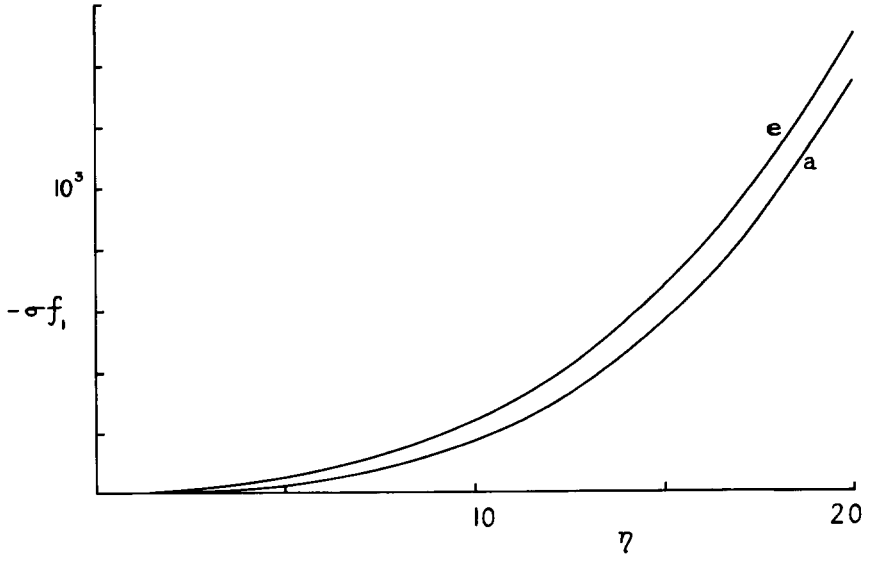

Fig. 3. The function f_1 for Prandtl numbers: (a) 0.028; (e) 17.2.

obtained from (6) and from matching with the small $-z$ expansion of (28) provided by (13). The required solution is

$$g_0 = \beta\eta\{1 - \Gamma(-\tfrac{1}{3}, 2\alpha\sigma\eta^3/9)/\Gamma(-\tfrac{1}{3})\} \tag{32}$$

and is shown in Fig. 4 for various values of the Prandtl number. At second order g_1 is found to satisfy

$$g_1'' + \tfrac{2}{3}\alpha\sigma\eta^2 g_1' - \tfrac{4}{3}\alpha\sigma\eta g_1 = \tfrac{1}{3}\sigma(f_1' g_0 - 3f_1 g_0'), \tag{33}$$

with boundary conditions

$$g_1' = 0 \quad (\eta = 0), \qquad g_1/\eta^2 \to 0 \quad (\eta \to \infty). \tag{34}$$

Solutions were obtained numerically by a Runge–Kutta scheme and are displayed in Fig. 5 for various values of the Prandtl number. The quadratic behaviour at infinity was avoided by computation of two solutions from the origin which were then used in the appropriate linear combination, giving

$$g_1 \sim a\beta/2\alpha \quad (\eta \to \infty). \tag{35}$$

This behaviour matches automatically with the outer solution

$$G_1 = aG_0'/2\alpha, \tag{36}$$

obtained from substitution of (28) into (3).

At large values of x the velocity field assumes the similarity form first found in [1], with

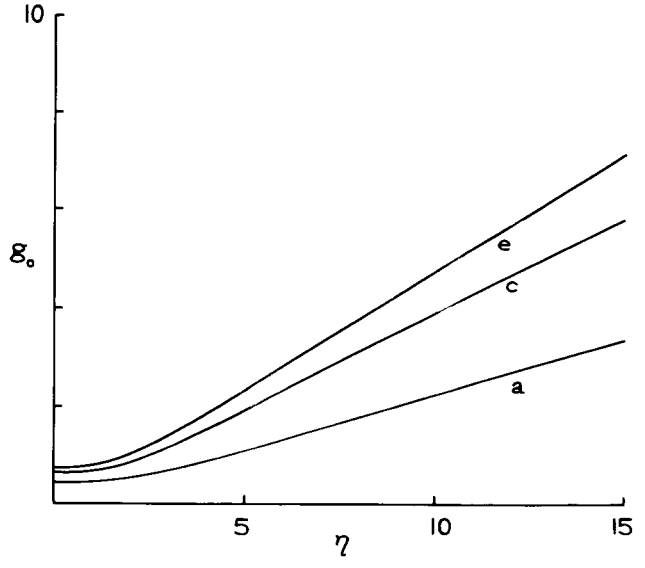

Fig. 4. The function g_0 for Prandtl numbers: (a) 0.028; (c) 0.72; (e) 17.2.

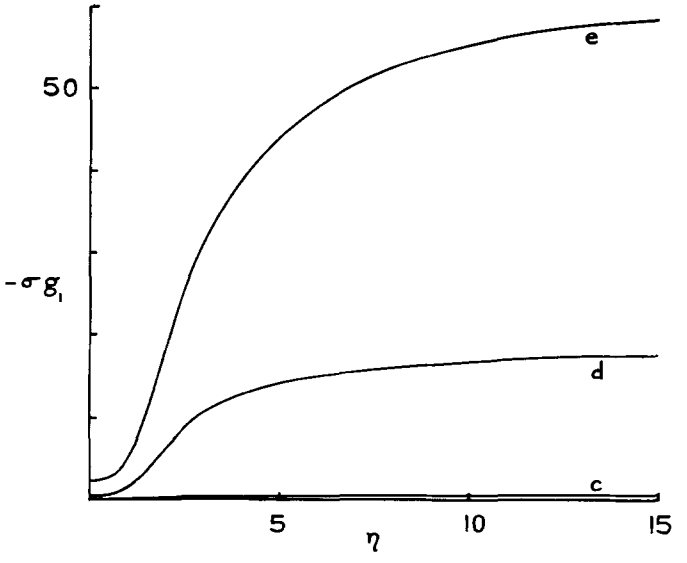

Fig. 5. The function g_1 for Prandtl numbers: (c) 0.72; (d) 8.1; (e) 17.2.

$$\psi \sim x^{1/4}\phi(\zeta) \quad (x \to \infty), \tag{37}$$

where $\zeta = z/x^{3/4}$. Here the scalings in x are dictated by equation (2) together with the integral relation (14), and ϕ satisfies

$$\phi''' + \tfrac{1}{4}\phi\phi'' + \tfrac{1}{2}\phi'^2 = 0, \tag{38}$$

$$\phi = \phi' = 0 \quad (\zeta = 0), \qquad \phi' \to 0 \quad (\zeta \to \infty), \tag{39}$$

with

$$\int_0^\infty \phi' \left\{ \int_\zeta^\infty \phi'^2 \, \mathrm{d}\zeta \right\} \mathrm{d}\zeta = P. \tag{40}$$

The required solution is

$$\phi = (40P)^{1/4}\Phi^2, \tag{41}$$

where

$$\tfrac{1}{4}(40P)^{1/4}\zeta = \ln \frac{(1 + \Phi + \Phi^2)^{1/2}}{1 - \Phi} + \sqrt{3} \tan^{-1} \frac{\sqrt{3}\Phi}{2 + \Phi}. \tag{42}$$

The heat-flux integral (15) now dictates that the temperature approaches its final constant form with an algebraic decay of order $x^{-1/4}$, so that

$$T \sim 1 - x^{-1/4}\theta(\zeta) \quad (x \to \infty), \tag{43}$$

where θ satisfies

$$\theta'' + \tfrac{1}{4}\sigma(\phi\theta' + \phi'\theta) = 0\,, \tag{44}$$

$$\theta' = 0 \quad (\zeta = 0)\,, \qquad \theta \to 0 \quad (\zeta \to \infty) \tag{45}$$

and

$$-\int_0^\infty \phi\theta'\,\mathrm{d}\zeta = Q\,. \tag{46}$$

The required solution is

$$\theta = \theta_0(1 - \Phi^3)^\sigma\,, \tag{47}$$

where

$$\theta_0 = Q\Gamma(\sigma + \tfrac{5}{3})/\{\Gamma(\sigma)\Gamma(\tfrac{5}{3})\sigma(40P)^{1/4}\}\,. \tag{48}$$

Further terms in the expansions (37) and (43) have not been investigated in detail although there are certainly correction terms of order $x^{-3/4}$ and $x^{-5/4}$ respectively, equivalent to an origin shift in x.

4. Numerical solution

A finite difference scheme was used to obtain numerical solutions of the system (1)–(8) for a range of values of the Prandtl number. The system is parabolic and solutions were computed by a downstream marching procedure, using Newton iteration to solve the discretized form of the nonlinear momentum equation at each x station. In view of the initial development of the jet outlined in Section 3, in $x < 1$ the equations were discretized onto inner and outer meshes which conformed with the asymptotic structure as $x \to 0$. For the inner mesh the solution is written as

$$\psi = \xi^2 A(\xi, \eta)\,, \qquad T = \xi D(\xi, \eta)\,, \tag{49}$$

where

$$\xi = x^{1/3}\,, \qquad \eta = z/x^{1/3}\,, \tag{50}$$

giving equations which may be expressed in first-order form as

$$\frac{\partial C}{\partial \eta} + \frac{2}{3}AC - \frac{1}{3}B^2 - \frac{1}{3}\xi\left(B\frac{\partial B}{\partial \xi} - C\frac{\partial A}{\partial \xi}\right) = 0\,, \tag{51}$$

$$\frac{1}{\sigma}\frac{\partial E}{\partial \eta} + \frac{2}{3}AE - \frac{1}{3}DB - \frac{1}{3}\xi\left(B\frac{\partial D}{\partial \xi} - E\frac{\partial A}{\partial \xi}\right) = 0\,, \tag{52}$$

where

$$C = \frac{\partial B}{\partial \eta}\,, \qquad B = \frac{\partial A}{\partial \eta}\,, \qquad E = \frac{\partial D}{\partial \eta}\,, \tag{53}$$

together with boundary conditions at the wall

$$A = B = E = 0 \quad (\eta = 0)\,. \tag{54}$$

For the outer mesh the solution is expressed as

$$\psi = \bar{A}(\xi, z)\,, \qquad T = \bar{D}(\xi, z)\,, \tag{55}$$

giving equations which may be expressed in first-order form as

$$\frac{\partial \bar{C}}{\partial z} = \frac{1}{3\xi^2}\left(\bar{B}\,\frac{\partial \bar{B}}{\partial \xi} - \bar{C}\,\frac{\partial \bar{A}}{\partial \xi}\right), \tag{56}$$

$$\frac{1}{\sigma}\,\frac{\partial \bar{E}}{\partial z} = \frac{1}{3\xi^2}\left(\bar{B}\,\frac{\partial \bar{D}}{\partial \xi} - \bar{E}\,\frac{\partial \bar{A}}{\partial \xi}\right), \tag{57}$$

where

$$\bar{C} = \frac{\partial \bar{B}}{\partial z}\,, \qquad \bar{B} = \frac{\partial \bar{A}}{\partial z}\,, \qquad \bar{E} = \frac{\partial \bar{D}}{\partial z}\,, \tag{58}$$

together with outer boundary conditions

$$\bar{B} \to 0\,, \qquad \bar{D} \to 1 \quad (z \to \infty)\,. \tag{59}$$

Initial profiles for the solution in the outer region are

$$\bar{A} = F_0\,, \qquad \bar{B} = F_0'\,, \qquad \bar{C} = F_0''\,, \qquad \bar{D} = G_0\,, \qquad \bar{E} = G_0' \quad (\xi = 0)\,, \tag{60}$$

and in the inner region

$$A = \alpha\eta^2\,, \qquad B = 2\alpha\eta\,, \qquad C = 2\alpha\,, \qquad D = g_0\,, \qquad E = g_0' \quad (\xi = 0)\,. \tag{61}$$

These equations and boundary conditions are now discretized using central differences and uniform steps $\Delta\xi$, $\Delta\eta$ and Δz. At a given downstream step ξ the inner mesh extends to $\eta = \eta_\infty$ while the outer mesh occupies $z_0 \leqslant z \leqslant z_\infty$ where $z_0 = \eta_\infty \xi$. The step lengths are chosen such that the outer mesh is reduced by one step in z for each downstream step in ξ, i.e. $\Delta z = \eta_\infty\,\Delta\xi$, in the manner described by Smith [18]. At the common boundary of the two regions continuity requires

$$\xi^2 A = \bar{A}\,, \qquad \xi B = \bar{B}\,, \qquad C = \bar{C}\,, \qquad \xi D = \bar{D}\,, \qquad E = \bar{E}\,. \tag{62}$$

Details of the discretized form of the system (51)–(54) and (56)–(62) and of the resulting matrix equation for the Newton increments associated with the momentum field at each downstream step are given in [16]; the solution at the previous step is used to provide an initial guess and convergence is required to within a specified tolerance. The linear system for the temperature then requires only a single solution of the appropriate matrix equation at each downstream step.

The choice $\Delta z = \Delta\eta$ ensures that at $x = 1$ grid points of the inner and outer meshes are spaced at equal intervals in z and a switch is made to a uniform mesh in

$$\chi = x^{1/4}, \qquad \zeta = z/x^{3/4}, \tag{63}$$

with

$$\psi = \chi\tilde{A}(\chi, \zeta), \qquad T = 1 - \chi^{-1}\tilde{D}(\chi, \zeta). \tag{64}$$

This ensures that the diffusing jet is adequately represented in the numerical scheme at large values of x. For $x > 1$ the system of first-order equations

$$\frac{\partial\tilde{C}}{\partial\zeta} + \frac{1}{4}(\tilde{A}\tilde{C} + 2\tilde{B}^2) - \frac{1}{4}\chi\left(\tilde{B}\frac{\partial\tilde{B}}{\partial\chi} - \tilde{C}\frac{\partial\tilde{A}}{\partial\chi}\right) = 0, \tag{65}$$

$$\frac{1}{\sigma}\frac{\partial\tilde{E}}{\partial\zeta} + \frac{1}{4}(\tilde{A}\tilde{E} + \tilde{B}\tilde{D}) - \frac{1}{4}\chi\left(\tilde{B}\frac{\partial\tilde{D}}{\partial\chi} - \tilde{E}\frac{\partial\tilde{A}}{\partial\chi}\right) = 0, \tag{66}$$

$$\tilde{C} = \frac{\partial\tilde{B}}{\partial\zeta}, \qquad \tilde{B} = \frac{\partial\tilde{A}}{\partial\zeta}, \qquad \tilde{E} = \frac{\partial\tilde{D}}{\partial\zeta}, \tag{67}$$

must be solved subject to the boundary conditions

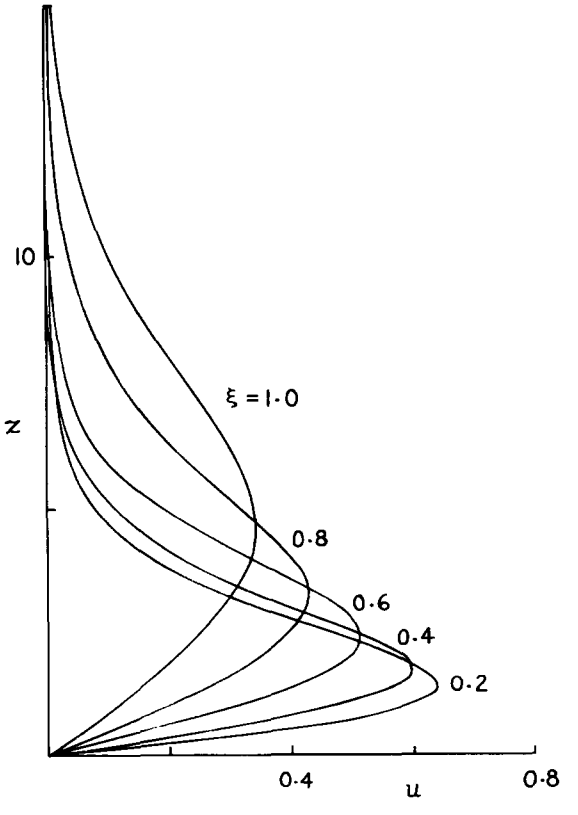

Fig. 6. Velocity profiles u for $\sigma = 0.72$ at $\xi = 0.2, 0.4, 0.6, 0.8, 1.0$.

$$\tilde{A} = \tilde{B} = \tilde{E} = 0 \quad (\zeta = 0), \tag{68}$$

$$\tilde{B} \to 0, \qquad \tilde{D} \to 0 \quad (\zeta \to \infty), \tag{69}$$

and initial conditions provided by the known profiles at $x = 1$. The system is discretized onto a uniform mesh in χ and ζ and at each downstream step the velocity field is found first using Newton iteration, allowing the temperature field to be obtained from a single solution of an appropriate matrix equation. Details of the discretized equations are given in [16].

Most computations were carried out with step sizes $\Delta\eta = \Delta z = \Delta\zeta = 0.1$, $\Delta\xi = 0.02$, $\Delta\chi = 0.1$, outer boundaries $\eta_\infty = 5$, $z_\infty = \zeta_\infty = 25$ and a tolerance of 10^{-4} for the Newton increments at each downstream step. Several checks were made on the accuracy of the calculations using different step sizes and also by evaluating the conserved integrals (14) and (15) at each downstream step. Some of the results are summarised in Table 2.

Complete downstream integrations were performed for several values of the Prandtl number. Figures 6–9 show velocity and temperature profiles at several locations in the jet and Fig. 10 shows the streamwise variation of the main properties of the flow for the case of air ($\sigma = 0.72$). The results were found to be in excellent agreement with the asymptotic forms obtained in Section 3.

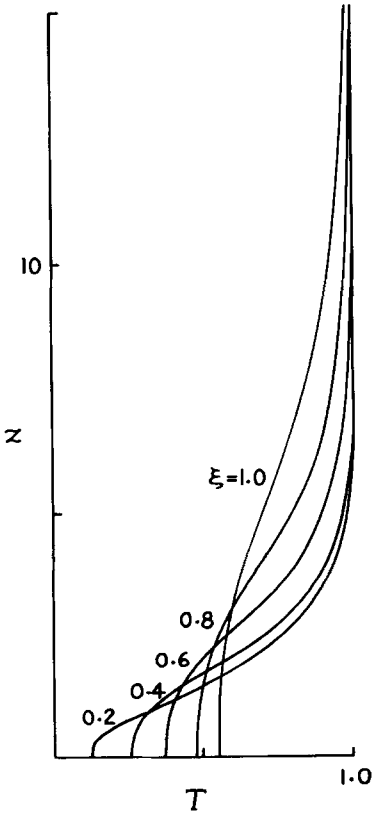

Fig. 7. Temperature profiles T for $\sigma = 0.72$ at $\xi = 0.2$, 0.4, 0.6, 0.8, 1.0.

Table 2. A selection of numerical results for different step sizes ($x \leqslant 1$) and $\sigma = 0.72$

$\Delta\eta = \Delta z = 0.2$, $\Delta\xi = 0.04$				
ξ	P	Q	$T(x, 1)$	$u(x, 1)$
0.2	0.6337	0.7112	0.3550	0.6114
0.6	0.6339	0.6949	0.3845	0.3020
1.0	0.6279	0.7036	0.5390	0.1053
$\Delta\eta = \Delta z = 0.1$, $\Delta\xi = 0.02$				
ξ	P	Q	$T(x, 1)$	$u(x, 1)$
0.2	0.6490	0.7171	0.3549	0.6111
0.6	0.6488	0.7171	0.3843	0.3024
1.0	0.6485	0.7170	0.5385	0.1058

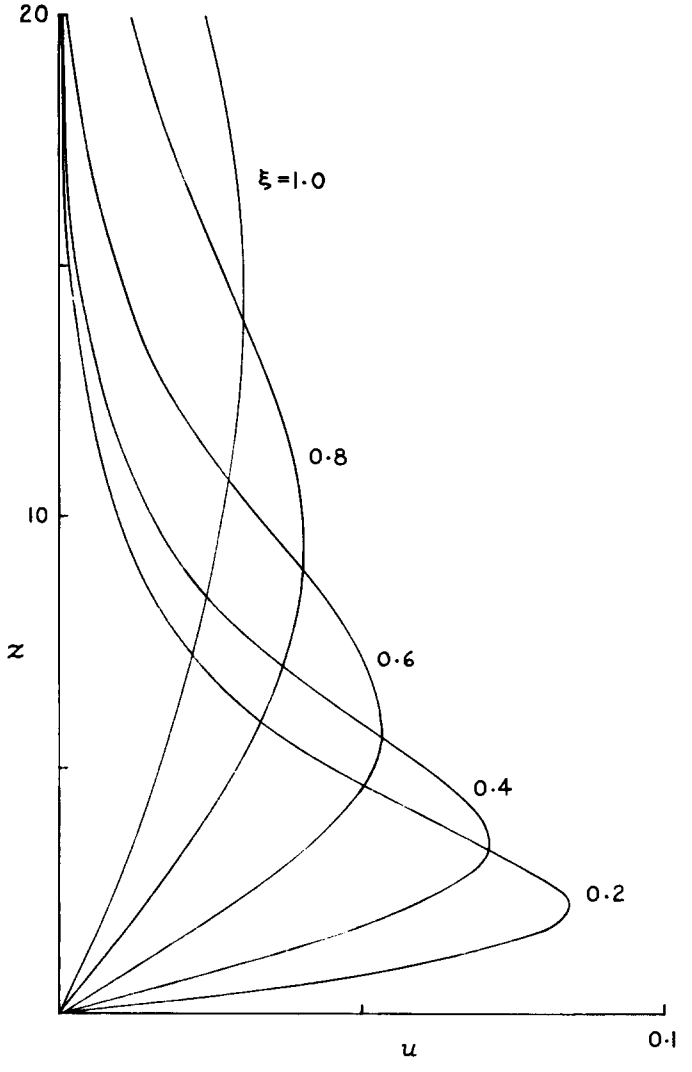

Fig. 8. Velocity profiles u for $\sigma = 8.1$ at $\xi = 0.2$, 0.4, 0.6, 0.8, 1.0.

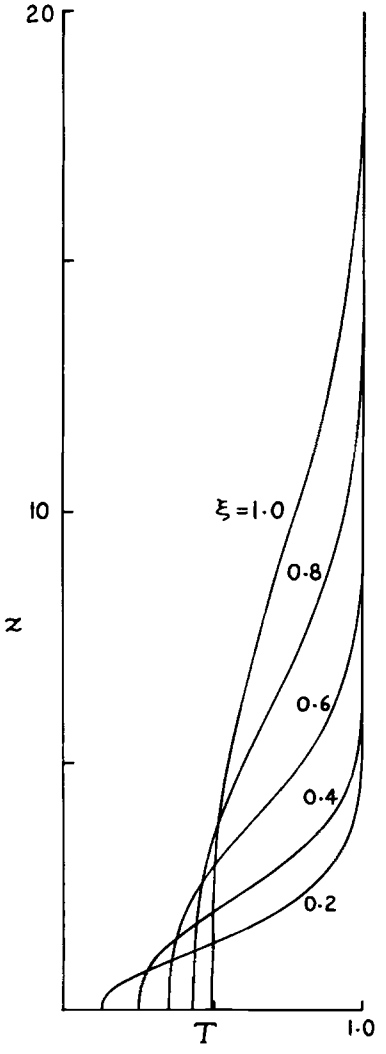

Fig. 9. Temperature profiles T for $\sigma = 8.1$ at $\xi = 0.2, 0.4, 0.6, 0.8, 1.0$.

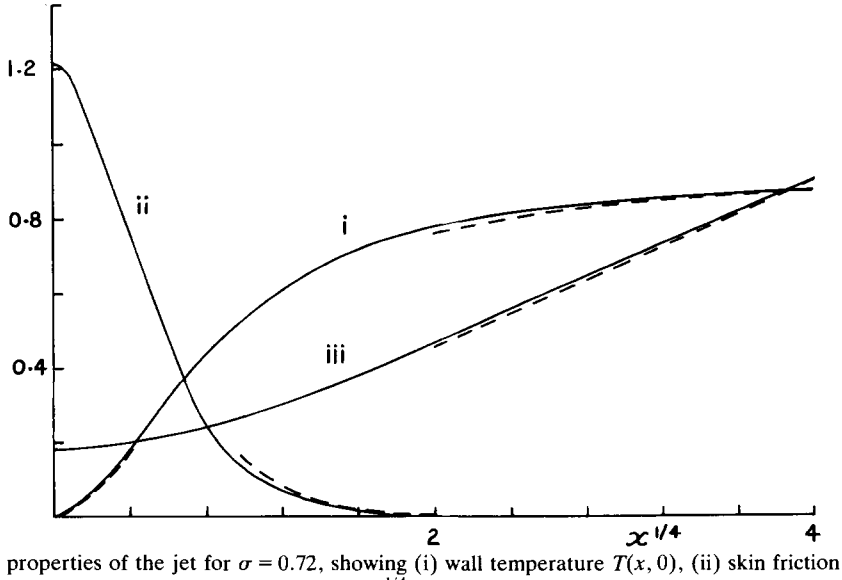

Fig. 10. Main properties of the jet for $\sigma = 0.72$, showing (i) wall temperature $T(x, 0)$, (ii) skin friction $\partial u/\partial z(x, 0)$ and (iii) stream function $\psi(x, \infty)/10$, as functions of $x^{1/4}$. Dashed curves indicate the asymptotes corresponding to (70)–(73).

5. Summary and discussion

The numerical results confirm the evolution of the jet into the form predicted by the asymptotic solution of Glauert [1] and the corresponding temperature field (43). As the jet proceeds downstream it entrains fluid, widens ($z \sim x^{3/4}$), slows down and assumes the uniform temperature of the ambient fluid. As $x \to \infty$, the wall temperature and skin friction are

$$T(x,0) \sim 1 - x^{-1/4}\theta_0 \,, \tag{70}$$

$$\frac{\partial u}{\partial z}(x,0) \sim x^{-5/4}(40P)^{3/4}/72 \,, \tag{71}$$

while at the edge of the jet

$$w(x,\infty) \sim -x^{-3/4}(40P)^{1/4}/4 \quad (x \to \infty) \,. \tag{72}$$

The initial evolution of the jet is characterised by a sudden adjustment of the wall temperature. Heat cannot escape through the wall or at the edge of the jet and so the temperature of the jet rises rapidly, with

$$T(x,0) \sim x^{1/3}\beta(2\alpha\sigma/9)^{-1/3}/\Gamma(\tfrac{2}{3}) \quad (x \to 0) \,, \tag{73}$$

at the wall. In the course of the flow all of the isotherms which enter the jet at $x = 0$ attach to the wall.

Figures 6–9 indicate the dependence of the flow on the Prandtl number of the fluid. At small Prandtl numbers the temperature adjusts on a scale much wider than that of the velocity field, while at large Prandtl numbers the reverse is true. For air, the results show that the jet attains its asymptotic form within a streamwise distance x^* of about $2^4(Uh/\nu)h$. Horizontal intrusions in shallow, thermally-driven cavity flows eventually give way to a second stage of evolution in which buoyancy comes into play, [11]. As the jet diffuses the inertial and viscous terms in the horizontal momentum equation (2) weaken relative to the effect of buoyancy, leading to a coupling of the thermal and velocity fields on a longer streamwise length scale. This second stage of evolution will be considered in future work.

One of us (RJG) is grateful to the Science and Engineering Research Council for support in the form of a Research Studentship.

References

1. M.B. Glauert, The wall jet. *J. Fluid Mech.* 1 (1956) 625–643.
2. D.T.J. Hurle, Temperature oscillations in molten metals and their relationship to growth striae in melt-grown crystals. *Phil. Mag.* 13 (1966) 305–310.
3. B.E. Boyack and D.W. Kearney, Heat transfer by laminar natural convection in low aspect ratio cavities. *ASME Paper* 72-HT-2 (1972).
4. A. Bejan and A.N. Rossie, Natural convection in a horizontal duct connecting two fluid reservoirs. *J. Heat Transfer* 103 (1981) 108–113.
5. D.E. Cormack, L.G. Leal and J. Imberger, Natural convection in a shallow cavity with differentially heated end walls. Part 1. Asymptotic theory. *J. Fluid Mech.* 65 (1974) 209–229.
6. P.G. Daniels, P.A. Blythe and P.G. Simpkins, Onset of multicellular convection in a shallow laterally heated cavity. *Proc. Roy. Soc. Lond.* A411 (1987) 327–350.
7. A. Bejan, A.A. Al-Homoud and J. Imberger, Experimental study of high Rayleigh number convection in a horizontal cavity with different end temperatures. *J. Fluid Mech.* 109 (1981) 283–299.

8. P.G. Simpkins and K.S. Chen, Convection in horizontal cavities. *J. Fluid Mech.* 166 (1986) 21–39.
9. S.G. Schladow, J.C. Patterson and R.L. Street, Transient flow in a side-heated cavity at high Rayleigh number: a numerical study. *J. Fluid Mech.* 200 (1989) 121–148.
10. J.C. Patterson and S.W. Armfield, Transient features of natural convection in a cavity. *J. Fluid Mech.* 219 (1990) 469–497.
11. P.G. Daniels, P.A. Blythe and P.G. Simpkins, High Rayleigh number thermal convection in a shallow laterally heated cavity, AT & T Bell Laboratories Tech. Mem. (1987, unpublished).
12. E. Pohlhausen, Der warmeaustausch zwischen festen korpern und flussigkeiten mit kleiner reibung und warmeleitung. *Z. Angew. Math. Mech.* 1 (1921) 115–121.
13. S. Goldstein, *Modern Developments in Fluid Dynamics*, Vol. 2, §273, Oxford University Press (1938).
14. F.T. Smith and P.W. Duck, Separation of jets or thermal boundary layers from a wall. *Q.J. Mech. Appl. Math.* 30 (1977) 143–156.
15. S. Ostrach, An analysis of laminar free convection flow and heat transfer about a flat plate parallel to the direction of the generating body force, N.A.C.A. Tech. Note 2635, Washington D.C. (1952).
16. R.J. Gargaro, Thermally-driven shallow cavity flows, Ph.D thesis, City University, London (1991).
17. H.K. Kuiken, An asymptotic solution for large Prandtl number free convection. *J. Eng. Math.* 2 (1968) 355–371.
18. F.T. Smith, Boundary-layer flow near a discontinuity in wall conditions. *I.M.A. J. Appl. Math.* 13 (1974) 127–145.